



Investigation of Effects of ZrO₂ Doping on Electrical Properties of Soda Lime Silicate Glasses Using Dielectric Spectroscopy

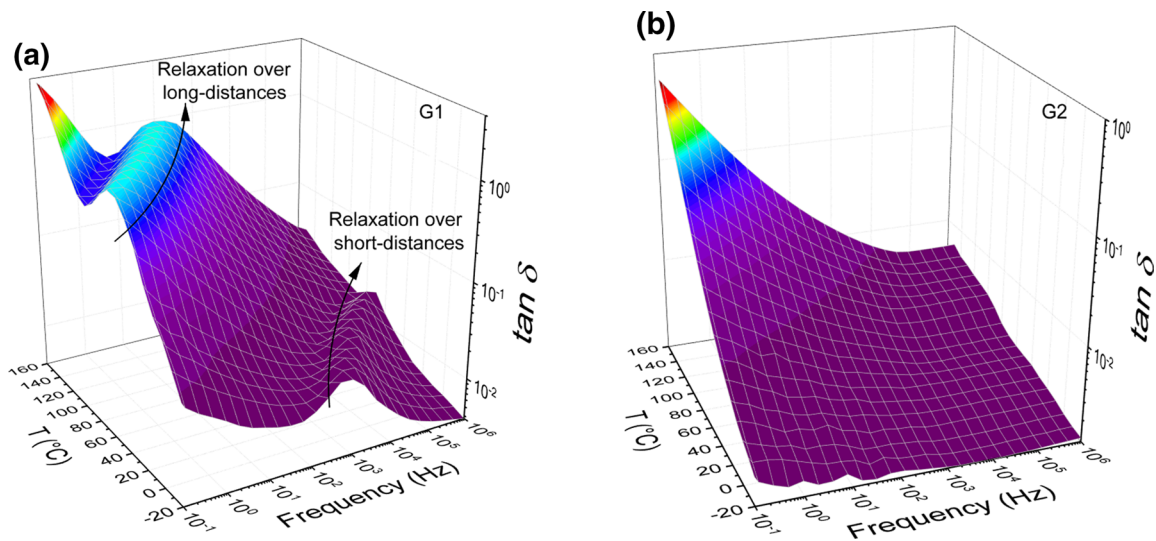
Chahira Ben Amara¹ · Helmi Hammami¹ · Slim Fakhfakh¹ · Ali Kallel¹

Received: 7 February 2021 / Accepted: 14 July 2021 / Published online: 26 July 2021
© The Minerals, Metals & Materials Society 2021

Abstract

The influence of the ZrO₂ doping content on the electrical and dielectric properties of soda lime silicate glasses has been investigated through the impedance spectroscopy technique based on dielectric measurements carried out in the frequency range from 0.1 MHz to 1 MHz at temperatures ranging between -20°C and 150°C . The experimental results depict an overall decrease in the electrical parameters [dielectric constant, loss, and alternating-current (AC) conductivity] when ZrO₂ was present in the soda lime glass, revealing a blockage of the easy pathways available for charge carrier (Na⁺) migration, subsequently yielding a reduction in their contribution to the space-charge polarization. This interpretation was also confirmed by the equivalent circuit suggested by ZView software. The resistivity actually increased with increasing ZrO₂ content. This result indicates that the internal structure of the soda lime silicate glass becomes more polymerized, electrically rigid, and resistant to the flow of free charge carriers in the presence of ZrO₂. Additional measurements using infrared (IR) spectroscopy were used to validate these findings.

Graphical Abstract



Keywords Soda lime silicate glass · dioxide zirconium (ZrO₂) · impedance spectroscopy · conductivity · resistivity · activation energy

✉ Slim Fakhfakh
slimfakhfakh@yahoo.fr

¹ LaMaCoP, Physics Department, Faculty of Sciences,
University of Sfax, Km 3, BP 1171, C.P 3000 Sfax, Tunisia

Introduction

In sodium silicate glasses, which exhibit outstanding properties, zirconium dioxide represents an intermediate oxide that can penetrate and increase their transparency, chemical inertness, and electrical resistivity, resulting in a reduction in the photochromism of such glasses and an enhancement of their optical properties and refractive index.^{1–4} For instance, zirconium dioxide (ZrO_2) is introduced into glass fibers as a consolidating element for cement products⁵ and as a nucleating agent in multiple glass–ceramics.^{6,7} Additionally, the presence of ZrO_2 in silicate glass matrices is deemed necessary to extend the transparency spectral range ($0.3\ \mu\text{m}$ to $8\ \mu\text{m}$).^{2,8,9} From this perspective, soda lime zirconium silicate represent another interesting class of metal-oxide glass materials (for example, the complex iron oxides,^{10,11} where various methods for obtaining complex oxide compound precursors are known.^{12,13} Their fields of application encompass optical devices, electrochemical capacitor electrodes, sensors, and fuel cells.^{14–17} Basically, these glasses are widely used as optical filters, laser mirrors, and alternative gate dielectrics in microelectronics.^{18,19}

It has been proven that addition of zirconia affects the properties of soda-lime silicate glasses, preventing the movement of modifier cations by increasing the diffusion energy barriers at both low and high temperature.²⁰ Furthermore, some studies based on molecular dynamics (MD) simulations^{21,22} have demonstrated that substitution of $\text{ZrO}_2/\text{SiO}_2$ has a remarkable effect on the structure of glasses. In fact, addition of ZrO_2 to the glass system has already been the focus of numerous works seeking to increase the alkali resistance of porous glass.^{20,23,24}

The main aim of the work presented herein is to identify the modification of the electrical properties of soda-lime silicate glasses in the presence of small amounts (wt.%) of ZrO_2 by using the dielectric spectroscopy technique. Therefore, electrical parameters [dielectric constant, loss, alternating-current (AC) conductivity, and impedance spectra] of two types of soda lime silicate glasses, viz. without (G1) and with ZrO_2 (G2), were investigated to analyze the impact of ZrO_2 on the dynamic properties of sodium ions. The experimental results reveal a different dielectric behavior related to the presence of ZrO_2 . In particular, a reduction in the contribution of the charge carriers was recorded, resulting in a reduction in the AC conductivity. This trend was verified by the equivalent circuit proposed by ZView software, where the resistivity value was determined for both glasses G1 and G2, with and without ZrO_2 content, respectively. Furthermore, spectral infrared absorption measurements on both glasses were carried out under the same condition to improve understanding of the effect of ZrO_2 on the

dynamic properties of sodium ions and therefore on network modification.

Experimental Procedures

Materials

The studied samples include two types of glasses: alkali silicate (G1) and alkali silicate with 2 wt.% ZrO_2 content (G2), in cylindrical form (1 mm thick, 10 mm in diameter) obtained from Saint-Gobain Research Company (Paris-Aubervilliers, France). Their chemical composition and physical characteristics (conductivity σ , relative dielectric constant ϵ_r , and density ρ) were provided by Saint-Gobain and are presented in Table I. The conductivity and relative dielectric constant were deduced from the voltage–current characteristic using a sample bias method at room temperature. The homogeneity of the glasses was assessed using electron probe microanalysis (EPMA) after metallization. Both sets of samples (G1 and G2) were transparent.

Role of the Elements in the Network of the Studied Glasses: Previous Studies

Generally, Si ions act as a fundamental element in a glass network, while Ca ions act as a network modifier that influences the structure of the glass by providing local load sites. Acting as both a network modifier and an intermediate, Al^{3+} can substitute for Si ions, thereby enhancing the encapsulation of the glass matrix and improving the acid resistance of the vitrified slag, provided that an adequate amount is added.^{25,26} In addition to CaO , Al_2O_3 , and SiO_2 , the presence of an alkaline oxide such as sodium oxide (Na_2O), for soda-lime glass, breaks Si–O–Si bonds and creates ionic bonds between the modifiers and the oxygen in the network. Following this rupture, oxygen that was initially a bridging oxygen (BO) becomes a nonbridging oxygen (NBO). NBOs result from negatively charged oxygens that no longer connect two silica tetrahedra. Depending on the type of modifiers used, i.e., monovalent or divalent, different mechanisms are activated. NBOs are created and distributed on the silica tetrahedra that basically form a fully connected network.^{27,28} However, a small number of Na^+ ions can decrease the number of NBO ions and increase the extent of aggregation in the $\text{CaO–Al}_2\text{O}_3\text{–SiO}_2$ system.²⁹ The presence of a small amount (wt.%) of ZrO_2 in the glass matrix triggers a decrease in the conductivity and substantially reduces the mobility of Na^+ ions.³⁰

Infrared Absorption Measurements

IR measurements were performed using a PerkinElmer Fourier-transform (FT)-IR spectrometer in the wavenumber range from 400 cm⁻¹ and 4000 cm⁻¹ with a 2-cm⁻¹ instrumental resolution. Quantitative analysis of the infrared spectra was conducted by careful deconvolution of the absorption profiles using the PeakFit program that takes into account masked peaks at wavenumbers that differ from the principal maximum in the infrared spectrum.

Electrical Measurements

Electrical measurements were conducted by impedance spectroscopy (IS) on both glasses (G1 and G2) in the frequency range from 0.1 MHz to 1 MHz in the temperature range from -20°C to 150°C at a rate of 10°C/min using a Novocontrol system based on an Alpha Analyzer with a temperature controller (Novocontrol quarto system controller BDS 1330). WinData and WinFit were used to enable the acquisition and processing of the resulting isochronal or isothermal spectra. WinFit software is essentially based either on the complex dielectric permittivity $\epsilon^*(\omega)$ in data processing or on the complex impedance $Z^*(\omega)$, which are related to each other by Eq. 1:

$$\epsilon^*(\omega) = \epsilon'(\omega) - j\epsilon''(\omega) = \frac{C^*(\omega)}{C_0} = -\frac{j}{\omega C_0 Z^*(\omega)} = \frac{Z''}{\omega C_0 (Z'^2 + Z''^2)} - j \frac{Z'}{\omega C_0 (Z'^2 + Z''^2)}, \quad (1)$$

where j is the square root of -1 , $C^*(\omega)$ is the complex capacity of the material under study, C_0 is the capacity of the empty sample capacitor, and $\omega = 2\pi f$ is the angular frequency.

$\epsilon'(\omega) = \frac{Z''}{\omega C_0 (Z'^2 + Z''^2)}$ and $\epsilon''(\omega) = \frac{Z'}{\omega C_0 (Z'^2 + Z''^2)}$ represent respectively the real and imaginary part of the dielectric permittivity ($Z^*(\omega) = Z'(\omega) - jZ''(\omega)$, where $Z'(\omega)$ and $Z''(\omega)$ are the real and imaginary parts of the complex impedance).

Results and Discussion

Infrared Spectral Analysis

The measured IR absorption spectra of the undoped and ZrO₂-doped soda lime silicate glass in the range from 400 cm⁻¹ to 4000 cm⁻¹ are depicted by Fig. 1. The spectral curves in the experimental IR data are generally identical or repetitive, indicating that the structural building units remain with only minor variations due to the low ZrO₂ doping level. The effect of ZrO₂ addition was explored by deconvolving the IR spectra using the PeakFit software. Several attempts were made using different band shapes until the best data fit was obtained, using Gaussian peaks. Based on the minimization of the deviations between the experimental and simulated spectra, the intensity, position, and full-width at half-maximum (FWHM) of each band were adjusted automatically by PeakFit. It Note that it is advantageous to limit the deconvolution procedure to the part of the spectrum in the range from 400 cm⁻¹ to 1300 cm⁻¹, which corresponds to the main structure of the silicate network. It is also beneficial to subtract the rest of the spectrum, which includes the bands caused primarily by water and OH groups.

Referring to Fig. 2a, b, eight peaks were observed after the deconvolution of the spectra for G1 and G2, respectively.

The extracted parameters (position, FWHM, and area) via the best fitting procedure are presented in Table II. As shown in Fig. 2a, b, the strong reflection band centered at around 476 cm⁻¹ refers basically to bending motions of the silicate tetrahedra. The two weak bands observed between 715 cm⁻¹ and 783 cm⁻¹ originate from inter-tetrahedral Si-O-Si vibrations. Moreover, the absorption peaks seen between 930 cm⁻¹ and 1155 cm⁻¹ may be resolved into three peaks, with one maximum (at 1030 cm⁻¹) and two shoulders (at ~ 940 cm⁻¹ and ~ 1140 cm⁻¹). The shoulder observed at nearly 940 cm⁻¹ is assigned to the asymmetric Si-O-NBO stretching mode, while the maximum and the other shoulder can be attributed to the asymmetric Si-O-Si stretching transverse optical mode and the asymmetric Si-O-Si

Table I Chemical composition (in wt.%) and physical characteristics of studied glasses (deduced by Saint-Gobain Research from voltage-current characteristic using a sample bias method)

Sample	Chemical Composition (in wt.%)					Physical Characteristics		
	SiO ₂	Al ₂ O ₃	Na ₂ O	CaO	ZrO ₂	σ (Ω ⁻¹ m ⁻¹)	ϵ_r	ρ (g cm ⁻³)
G1	72	0.3	13	15	0	10.2×10^{-12}	6.5	2.50
G2	73	0.4	9	16	2	0.67×10^{-12}	4.4	2.64

stretching longitudinal optical mode, respectively.^{31,32} Note that the position of the Si–O–Si band changes according to the amount and type of modifier cations introduced into the system.^{31,32} Thus, the creation of some vacancies and probably some substitution for hydrogen may result from the movement of sodium ions induced by the electric field. The alteration of the Si–O–Si-related band to higher wavenumber is in good agreement with the decrease in the alkali content of the G2 glass composition.^{33,34} The change in the position of the high-wavenumber peak at 1050 cm^{-1} in the IR reflection band is associated with a change in the glass structure.²⁸ As outlined in Fig. 2b, addition of ZrO_2 substitute for SiO_2 into the G2 glass shifted the peak situated at 1140 cm^{-1} towards a higher wavenumber of 1155 cm^{-1} . This shift indicates that ZrO_2 acts as a network former, reconnects the network break of glass, reduces the number of NBOs, decreases the specific volume, and improves the connectivity of the structure.

Dielectric Studies

The variation of the dielectric constant $\epsilon'(\omega)$ for both studied glasses displays an increasing trend with increasing temperature, particularly at lower frequencies (Fig. 3a, b). This increase is more obvious for glass G1, being associated with hopping conduction owing to the mobile charge carriers (Na^+) over long distances.³⁵ Indeed, the increase in $\epsilon'(\omega)$ occurs at higher temperatures and is more substantial at lower frequencies, where easy transport of conducting species is quite possible in the bulk sample. With the increase in the logarithmic frequency, the dielectric constant values decrease progressively for both glasses.³⁶ This trend may be related to the inability of charge carriers to rotate rapidly (or follow the electric field), thus producing a lag between the oscillation of the dipoles and the applied field.³⁵

Besides, we recorded a decrease in the permittivity, $\epsilon'(\omega)$, at each frequency and temperature with increasing ZrO_2 content in glass G2. This may be associated with the degree of polymerization of the glass network, which increases in parallel with the increase of tetrahedral zirconium ions.^{21,37,38} Consequently, easy pathways available for migration of charge carriers (Na^+) were blocked.³⁸ Hence, the contribution of the charge carriers to the space-charge polarization decreases and a reduction of $\epsilon'(\omega)$ with increasing ZrO_2 content was observed (Fig. 3b). In fact, glass G2 is composed of pathways rich in alkalis with isolated regions rich in silica. Adding zirconia can adjust this structure and make it less well connected. This reduction can be considered as an analogous charge compensation mechanism induced by the presence of zirconium, which causes a reduction of the amount of NBOs, as indicated above by the IR measurements.

The stoichiometry is particularly important for oxide compounds, and it is well known that complex compounds

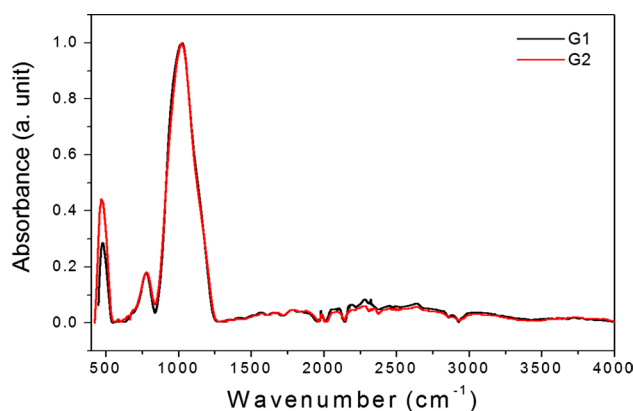


Fig. 1 IR absorption spectra of soda lime silicate glasses in undoped (G1) stated and when doped with zirconium dioxide (G2).

of transition metals easily allow excess and/or deficit of oxygen and can lead to phase separation of the crystal structure.³⁹ In addition, a deviation of the concentration of the original cations from a given value can lead to a change in the charge state of the cations. In turn, this greatly changes the magnetic and electrical parameters and seriously affects the practical application of the obtained materials.^{40,41} Furthermore, the average crystallite size can affect the dielectric properties of the obtained composites.^{42,43} Previous work⁴⁴ has showed that addition of even a low weight percentage of zirconium as in the current study (2 wt.%) to a similar system ($\text{Na}_2\text{O}-\text{CaO}-\text{Al}_2\text{O}_3-\text{SiO}_2$) does not result in any form of reactive disturbance such as phase separation or crystallization. Indeed, addition of ZrO_2 leads to a decrease in the number of $\text{Q}^3(\text{Si})$ units (silicon bridges with three network formers and one NBO oxygen linked to a network modifier) in favor of Si–O–Zr bonds designated as $\text{Q}^3(\text{Zr})$ (where Zr acts as a network former). This reduction is correlated with the increase in $[\text{ZrO}_6]^{2-}$ sites, which indicates a structural change in the role of Na^+ . Initially associated with the non-bridging oxygen of SiO_4 polyhedra, Na^+ becomes associated with $[\text{ZrO}_6]^{2-}$ sites as a charge compensator. Thus, the Na^+ ions change their role from network modifiers around $\text{Q}^3(\text{Si})$ to charge compensators, associated with negative charges around octahedral zirconium sites. An increase in the network polymerization is thus obtained. In conclusion, at low ZrO_2 content, sufficient Na and Ca are available to provide charge compensation around Zr sites, thus the stoichiometry of the oxygen atoms remains unchanged.

The dielectric loss, which reflects the energy loss in a material specimen as a function of the frequency of the applied electric field, can be calculated as follows (Fig. 4a, b):

$$\tan(\delta) = \frac{Z'}{Z''} = \frac{\epsilon''}{\epsilon'}. \tag{2}$$

Generally, the dielectric loss factor increases with temperature but decreases with increasing frequency, revealing different relaxation processes. At the beginning, in the low frequency region, an increase of the loss tangent can be assigned to the dominance of an ohmic (active)

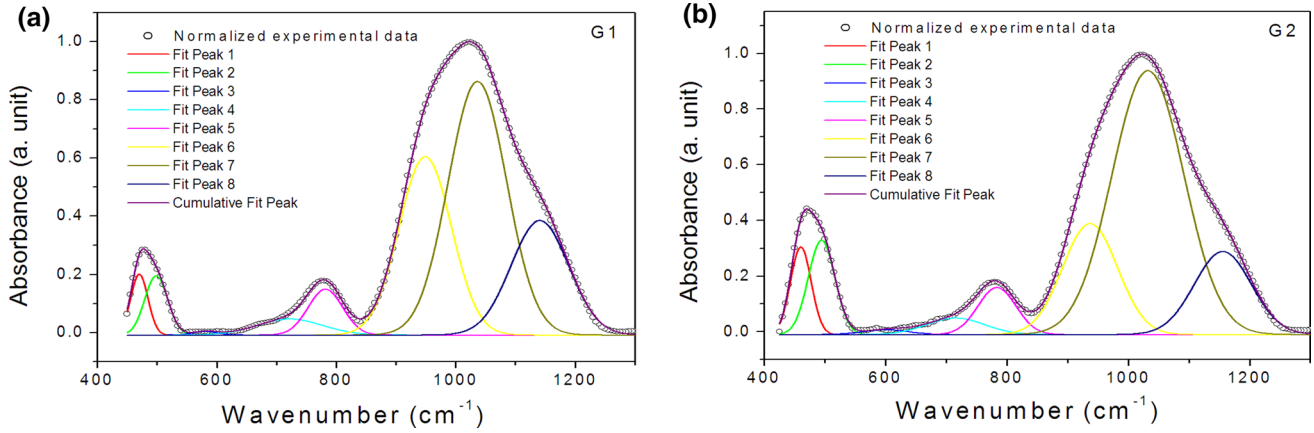


Fig. 2 Typical deconvolution of IR spectrum of soda lime silicate glasses: (a) undoped G1 and (b) doped with zirconium dioxide G2.

Table II Band center, FWHM, and area of deconvoluted peaks of soda lime silicate glass when undoped (G1) and doped with zirconium dioxide (G2)

	Peak	1	2	3	4	5	6	7	8
G1	Position	470	498	580	722	781	948	1036	1140
	FWHM	29	38	41	110	58	88	97	97
	Area	7	9	1	7	11	68	106	48
G2	Position	460	494	600	715	783	936	1032	1155
	FWHM	34	43	74	95	63	90	118	94
	Area	13	19	2	7	13	45	41	35

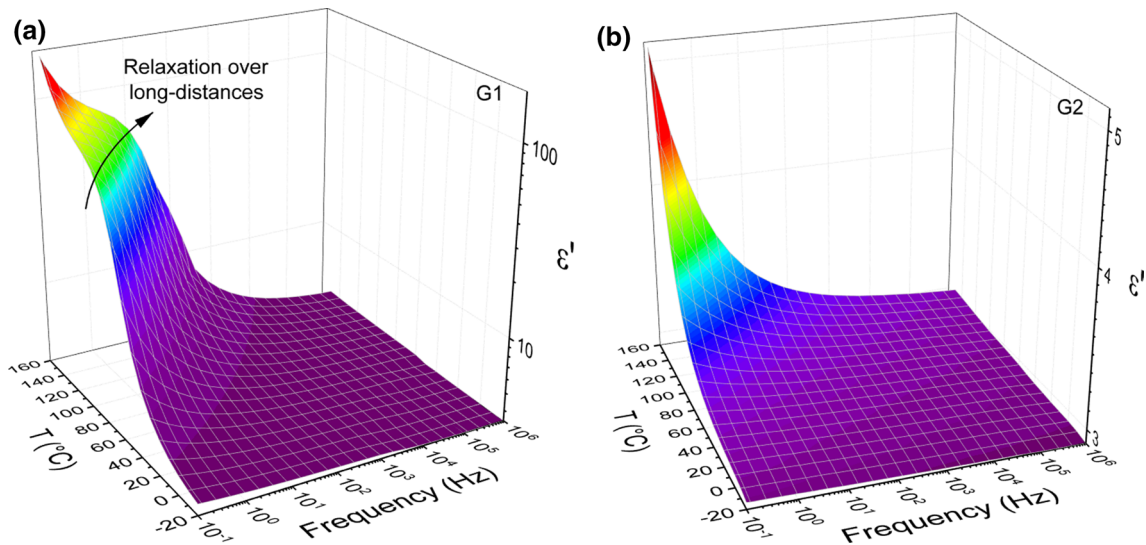


Fig. 3 Frequency dependence of dielectric constant ϵ' for glasses (a) G1 and (b) G2 at different temperatures from -20°C to 150°C in steps of 10°C .

component rather a capacitive component (reactive). When the frequency increases, the dipoles increasingly become unable to follow the oscillations of the electrical field, leading to a reduction in $\tan(\delta)$. However, no relaxation effects are detected in the plot for G2. Moreover, the dielectric loss is higher at lower frequency for G1 than G2, being related basically to the contribution of ion (Na^+) jumps in G1 and the decreased conductivity in G2.

At high frequency, mobile charge carriers (Na^+ , Ca^{2+}) can create bonds with the closest nonbridging oxygen to the volume, giving rise to a relaxation process that occurs over short distances and depends on the concentration of Na_2O . This process is only substantial in G1 but almost absent in G2. The low dielectric loss value implies that the structure of glass G2 is more stable. Indeed, the sodium ions can perform two roles in glass G2, acting as charge compensators around $(\text{ZrO}_6)^{2-}$ units^{20,38,45} or as network modifiers since the introduction of ZrO_2 can induce formation of strong Zr-O-Si bonds and therefore the movement of more Na^+ ions from a modifier position (close to NBOs) to a charge compensator position close to $(\text{ZrO}_6)^{2-}$ units. In reality, given the strong electrostatic attraction between NBO atoms and Na^+ ions, the compatibility of Zr-O with the silicate network (Si-O) increases enormously, thus leading to the development of strong Zr-O-Si bonds in the structure of glass G2, as confirmed by the IR spectroscopy analysis above. Furthermore, the presence of Zr-O-Si bonds in the structure of glass G2 minimizes the network alteration and prevents neighboring Si atoms from dissolving. In this glass, which contains mainly calcium as a charge compensator, the Zr-O-Si linkages are mostly or completely charge compensated by Ca^{2+} ions, which have higher field strength than Na^+ ions. These Ca^{2+} ions cause a lengthening of the Zr-O distance, which is

most likely to be associated with an increase in the average coordination number.

The low values of the dielectric constant and loss factor at higher frequency for the samples are key not only for the extension of the applications of such materials towards the photonic and electrooptic fields but also for their fundamental use as nonlinear optical materials.^{46,47} Basically, the combination of compounds with different electronic properties is accompanied by an evolution of the electrical characteristics and leads to new composite materials of great technological interest for industrial applications.^{48,49} In addition, these dielectric materials can be integrated as an important part of radiofrequency transceiver devices for mobile communications systems. However, the microwave properties of the material are determined by the dielectric and magnetic contributions. For such applications, it is more profitable to use dielectrics in addition to magnetodielectrics.^{50,51}

Electrical Conductivity Analysis

The electrical conductivity of most oxide glasses derives from ionic motion. Organic glasses can either be electronic conductors (Fe^{2+}) or exhibit ionic conduction resulting from impurities (Na^+). The most basic parameter associated with macroscopic measurements of the microscopic movement of charge carriers is the complex conductivity, expressed as

$$\sigma^*(\omega) = \sigma' + j\sigma'' \quad (3)$$

where $\sigma' = \omega\epsilon_0\epsilon'' = \omega\epsilon_0\epsilon'\tan(\delta)$ is the real part and $\sigma'' = \omega\epsilon_0\epsilon'$ is the imaginary part of the conductivity.

Figure 5a and b show plots of σ' versus frequency and temperature for G1 and G2, respectively.

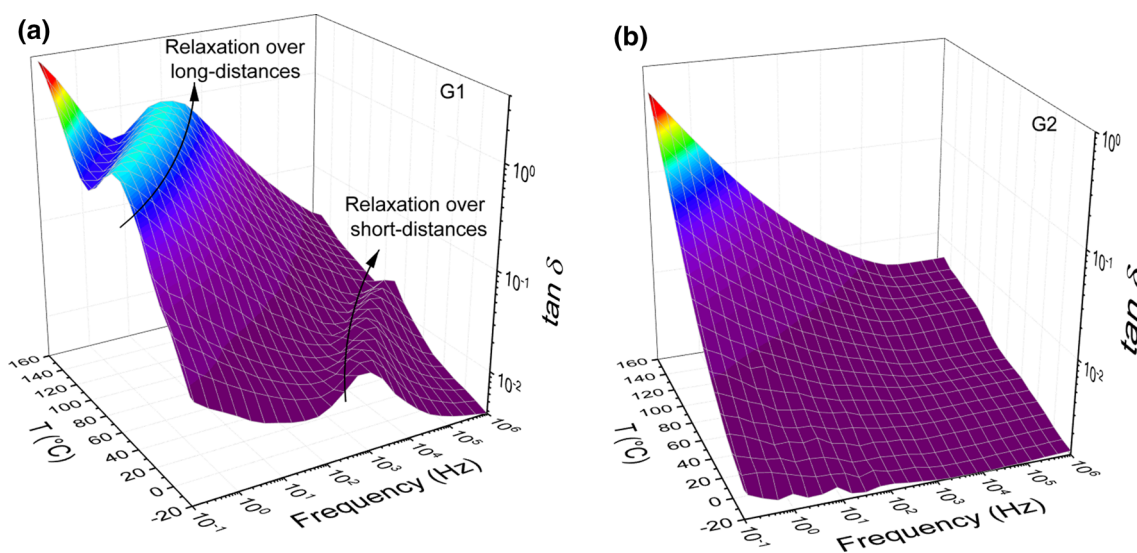


Fig. 4 Dielectric loss $\tan(\delta)$ as function of frequency for glass (a) G1 and (b) G2 at temperatures from -20°C to 150°C in steps of 10°C .

The low-frequency plateau seen for glass G1 corresponds to the direct-current (DC) conductivity σ_{DC} , which reflects the long-range transport of mobile ions (Na⁺) in the glass. The conductivity dispersion at frequencies between 0.1 Hz and 10³ Hz and temperatures above 50°C is related to correlated forward and backward hopping of ions.⁵² Therefore, more mobile cations (Na⁺) can now displace over larger distances via the hopping process.³⁵ With increasing temperature, an increasing concentration of Na⁺ cations move towards the cathode and away from the anode, which increases the sample polarization resulting from the increase in the bond charge density.

Moreover, it is noteworthy that the DC conductivity in the presence of ZrO₂ decreases by a few orders of magnitude (Fig. 5a, b). This considerable change in the DC conductivity can be assigned to the classic mixed mobile ions effect (MMIE) arising from the presence of different mobile ions (Na⁺ and Zr⁴⁺) in the glass structure.^{20,53} In fact, Zr⁴⁺ ions prove to be located at (ZrO₆)²⁻ sites, connected to the silicate network, and preferentially charge compensated by Na⁺ ions.^{20,38} In addition, the presence of Zr ions hinders the motion of Na⁺ ions, resulting in the reduction of the AC conductivity caused by the formation of strong Zr–O–Si bonds (see “Infrared Spectral Analysis” section). Note also that substitution of Si by Ca cation affects the mobility of the Na⁺ ions and blocks their diffusion. From this perspective, glass G2 acquires further electrical resistivity due to the higher concentration of calcium oxides.

Furthermore, the low values of electrical conductivity in glass G2 can be explained by the electrical conductivity definition in terms of the charge q , concentration n , and mobility μ of the carriers, according to the classical relation⁵⁴

$$\sigma = qn\mu. \quad (4)$$

Thus, this decrease is basically related to the mobility of the charge carriers. It is well known that this mobility depends on the temperature and glass composition.⁵⁴ At higher temperatures, the network’s thermal agitation reduces the carrier drift speed and thus mobility μ .⁵⁵ The presence of Zr⁴⁺ ions in glass G2 is expected to obstruct the displacement of the Na⁺ charge carriers and leads to a supplementary reduction in the conductivity resulting from the reduction of mobility. Indeed, addition of alkaline oxides to any glass former leads to a significant (many orders of magnitude) increase in the cationic conductivity of the glass. The presence of a low content of alkaline-earth oxide accompanied by a decrease in the alkali oxide (Na₂O) content (as in glass G2) leads to a decrease in the AC conductivity (Fig. 5b). Hence, the G2 composition exhibits the lowest values of conductivity compared with glass G1.

Nyquist Diagram and Equivalent Circuit

Exploring the variation of the impedance with frequency and temperature can provide useful information on the change in the bulk resistance of the glass samples. The impedance of the samples is a complex quantity represented by

$$Z^*(\omega) = Z'(\omega) - jZ''(\omega). \quad (5)$$

In Eq. 5, the real part Z' of the complex impedance represents the purely resistive component, while the imaginary part Z'' stands for the capacitive reactance of the sample. To determine the bulk resistance, relaxation time, and activation energy, the variations of the imaginary part of the complex impedance (Z'') versus the real part of impedance (Z') for both glasses are presented on a log–log (Nyquist) plot in Fig. 6a, b.

Theoretical curve fitting was carried out using ZView software, which is essentially designed for plotting and analysis of impedance data, fitting common circuits instantly, and offering best-in-class equivalent circuit modeling.⁵⁶ The obtained fit theoretical curves are in good agreement with the experimental data. It is fruitful to exploit an equivalent circuit model that allows a realistic representation of the electrical properties of the respective regions. Therefore, each semicircle is represented by a parallel RC element.^{57,58} In our case, the capacitor C is substituted by a constant-phase element (CPE), since each semicircle is deformed and its center is positioned below the Z' axis.

The plot for glass G1 comprises two arcs (Fig. 6a): one in the low-frequency region that corresponds to the electrode–glass interface, and one in the high-frequency region that corresponds to bulk phenomena. For glass G2, the diagrams in Fig. 6b display more open circular curves, where the different zones delimited gradually decrease as the temperature is increased, resulting in strong localization of charge carriers and an increase in the bulk resistance of G2. The dip in the plots in Fig. 6b corresponds to the minima in the imaginary part of the impedance denoting the bulk resistance (R_1) value (real part of impedance on the x -axis). Note also from Fig. 6a, b that the obtained diameter of the semicircles decreases greatly as the temperature is increased, which leads to a decrease in the resistivity and promotes an increase in the ionic conductivity.³⁵

The complex impedance plot for the G1 composition displays lower values of resistivity at given temperature compared with G2. This yields a rise in the resistivity in the presence of ZrO₂. This interesting situation results from the fact that the electrical resistance (the value of Z' at $Z'' = 0$ in the low frequency range) of glass G2 (the Zr-containing glass) is significantly higher than that of glass G1 (without Zr), as depicted in Tables III and IV, where the obtained parameters R_1 , R_2 , CPE₁, CPE₂, p_1 , and p_2

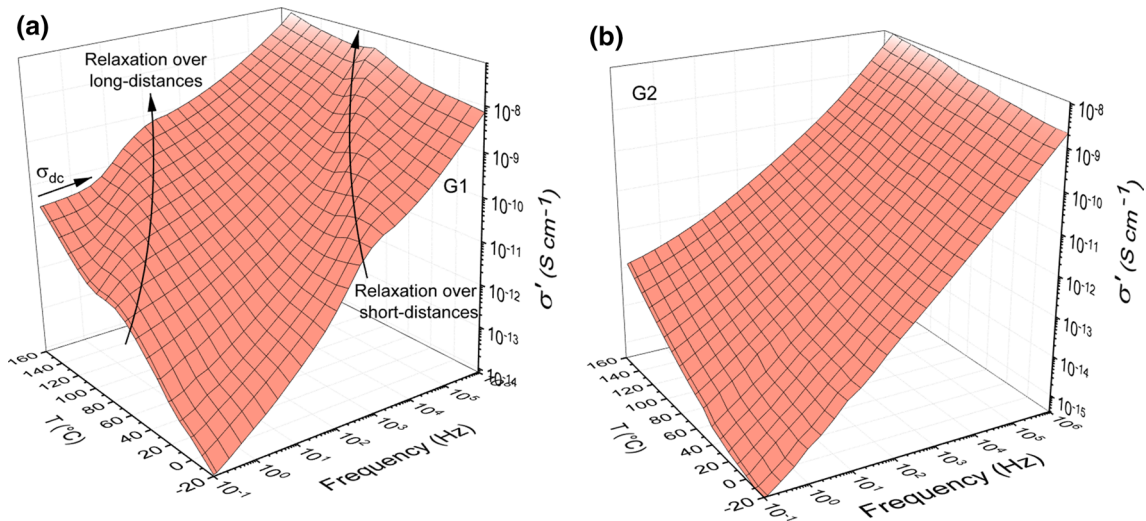


Fig. 5 Frequency dependence of conductivity at various temperatures for glass (a) G1 and (b) G2.

are presented. This can be attributed to the fact that the Zr cation blocks the displacement of the more mobile Na⁺ ions in the same way as Ca²⁺ ions do in the main soda lime silica glasses.⁵⁹ This result clearly confirms that the internal structure of glass G2 is more polymerized, electrically rigid, and resistant to flow of free charge carriers.

To identify the relaxation time τ at each temperature, the following relation was used:

$$\tau = (R \text{ CPE})^{\frac{1}{p}}, \tag{6}$$

where the parameter p reflects the deviation from ideal Debye behavior and takes a value of 0 for a pure resistor and 1 for a pure capacitor.

The evolution of the relaxation time against $1000/T$ is plotted in Fig. 7. The used Arrhenius model is expressed as

$$\tau = \tau_0 \exp\left(\frac{E_a}{K_B T}\right), \tag{7}$$

where τ_0 is the preexponential factor, E_a is the activation energy, T is the temperature in Kelvin, and K_B is the Boltzmann constant.

The values obtained for the activation energy E_a from these curves are presented in Fig. 7. The activation energy decreases in the silicate glass G2. In fact, the presence of ZrO₂ at low content gives rise to strong Zr–O–Si bonds following the combination of Zr⁴⁺ ions mainly in the form of ZrO₆ octahedra,⁴⁵ which makes the structure of glass G2 more rigid, enormously weakening the mobility of charge carriers (Na⁺, Ca²⁺). For glass G1 (without ZrO₂), the Na⁺ ions act as a modifier of the glass network by breaking Si–O–Si bonds and generating coordinated defects called NBOs. Consequently, the disorder in the glass structural network increases and the activation energy increases.

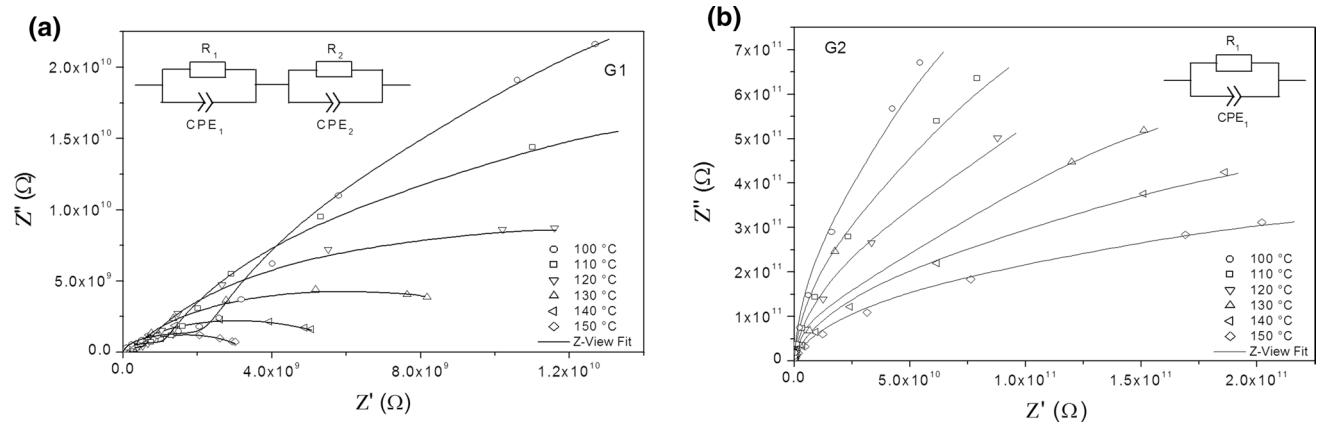


Fig. 6 Impedance diagrams for glass (a) G1 and (b) G2 at different temperatures. Inset shows corresponding equivalent circuit.

Table III Best-fit values of equivalent circuit elements in Fig. 6a for glass G1 at different temperatures

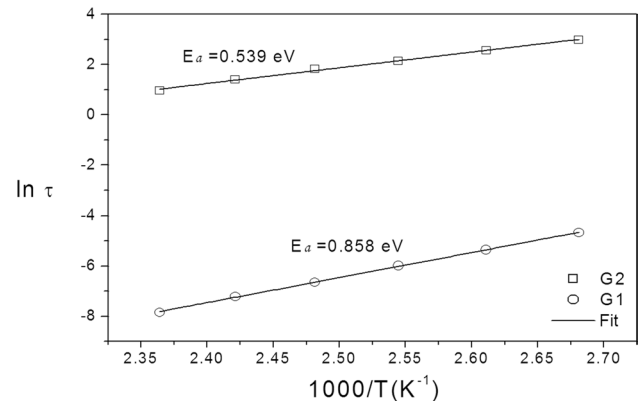
T (°C)	CPE_1 (F)	p_1	R_1 (Ω)	CPE_2 (F)	p_2	R_2 (Ω)
100	5.78×10^{-12}	0.95	2.05×10^9	5.57×10^{-11}	0.89	8.10×10^{10}
110	6.11×10^{-12}	0.95	1.02×10^9	6.07×10^{-11}	0.88	4.15×10^{10}
120	6.49×10^{-12}	0.95	5.24×10^8	6.65×10^{-11}	0.88	2.06×10^{10}
130	7.31×10^{-12}	0.95	2.60×10^8	7.82×10^{-11}	0.86	1.10×10^{10}
140	7.70×10^{-12}	0.95	1.37×10^8	8.78×10^{-11}	0.85	0.58×10^{10}
150	8.06×10^{-12}	0.94	7.88×10^7	9.34×10^{-11}	0.84	0.32×10^{10}

Table IV Best-fit values of equivalent circuit elements in Fig. 6b for glass G2 at different temperatures

T (°C)	CPE_1 (F)	p_1	R_1 (Ω)
100	2.26×10^{-12}	0.99	8.51×10^{12}
110	2.35×10^{-12}	0.99	5.37×10^{12}
120	2.50×10^{-12}	0.98	3.25×10^{12}
130	2.76×10^{-12}	0.97	2.13×10^{12}
140	3.08×10^{-12}	0.96	1.26×10^{12}
150	3.38×10^{-12}	0.95	0.74×10^{12}

Conclusions

Complex impedance spectroscopy revealed that addition of ZrO₂ affects the structural, dielectric, and electrical properties of soda lime silicate glass (G2). The results demonstrate that ZrO₂ acts as a glass former and reduces the number of NBOs, causing an improvement of the connectivity of the glass structure, as also confirmed by IR spectroscopy analysis. The obtained decrease of electric parameters (dielectric constant, loss, and Ac conductivity) in glass G2 compared with G1 indicates increased electrical rigidity in the soda lime silicate glass after addition of ZrO₂. This can be attributed to the predominant participation of Zr ions in tetrahedral and substitutional octahedral positions, resulting in a decrease in the concentration of free charge carriers as well as progressive blocking of the pathways for transport of conducting ions. The electrical properties of the glass samples (G1 and G2) are also confirmed by the equivalent circuit suggested by ZView software, where an increase in the resistivity with addition of ZrO₂ is noted. The current work constitutes could be extended and built upon. In fact, the promising glass G2 seems to be extremely useful for a wide range of applications. Indeed, in practice, such glasses may be beneficial for use in visible lasers for optical data storage systems. In addition, thanks to its high electrical resistance, glass G2 also has worthwhile applications in the electronics industry as an alternative grid dielectric.

**Fig. 7** Relaxation time versus inverse temperature for glasses G1 and G2. E_a is the activation energy.

Acknowledgment The authors thank Dr. D. Martin from Saint-Gobain Company (Aubervilliers, France) for providing samples.

Declarations

Conflict of interest The authors declare that they have no conflicts of interest. All authors confirm that they have no known competing financial interests or personal relationships that could have appeared to influence the results reported in this paper.

References

- H. Li, D. Wang, Meng, and C. Chen, *Biointerphases* 9, 031014 (2014).
- E.M.M. Ewais, M.A.A. Attia, A. Abousree-Hegazy, and R.K. Bordia, *Ceram. Int.* 36, 1327 (2010).
- A. Sawa, K. Nakanishi, and T. Hanada, *Thin Solid Films* 516, 4665 (2008).
- D. Tauch and C. Rüssel, *J. Non-Cryst. Solids* 353, 2109 (2007).
- V.T. Yilmaz, E.E. Lachowski, and F.P. Glasser, *J. Am. Ceram. Soc.* 74, 3054 (1991).
- O. Dargaud, G. Calas, L. Cormier, L. Galois, C. Jousseume, G. Querel, and M. Newville, *J. Am. Ceram. Soc.* 93, 342 (2010).
- O. Dargaud, L. Cormier, N. Menguy, L. Galois, G. Calas, S. Papin, G. Querel, and L. Olivi, *J. Non-Cryst. Solids* 356, 2928 (2010).

8. H. Yang, S. Wu, J. Hu, Z. Wang, R. Wang, and H. He, *Mater. Des.* 32, 1590 (2011).
9. S. Banijamali, B.E. Yekta, H.R. Rezaie, and V.K. Marghussian, *Thermochim. Acta* 488, 60 (2009).
10. S.V. Trukhanov, A.V. Trukhanov, V.G. Kostishyn, L.V. Panina, V.A. Turchenko, I.S. Kazakevich, A.V. Trukhanova, E.L. Trukhanov, V.O. Natarov, and A.M. Balagurov, *J. Magn. Magn. Mater.* 426, 554 (2017).
11. A.L. Kozlovskiy, I.E. Kenzhina, and M.V. Zdorovets, *Ceram. Int.* 46, 10262 (2020).
12. I.O. Troyanchuk, D.D. Khalyavin, S.V. Trukhanov, and H. Szymczak, *J. Phys. Condens. Matter.* 11, 8707 (1999).
13. M.V. Zdorovets, and A.L. Kozlovskiy, *J. Alloys Compd.* 815, 152450 (2020).
14. M. Salavati-Niasari, M. Dadkhah, and F. Davar, *Polyhedron* 28, 3005 (2009).
15. M. Salavati-Niasari, M. Dadkhah, and F. Davar, *Inorg. Chim. Acta* 362, 3969 (2009).
16. D.S. Patil, K. Prabhakaran, R. Dayal, C. Durga Prasad, N.M. Gokhale, A.B. Samui, and S.C. Sharma, *Ceram. Int.* 34, 1195 (2008).
17. Y.W. Zhang, J.T. Jia, C.S. Liao, and C.H. Yan, *J. Mater. Chem.* 10, 2137 (2000).
18. D. Panda, and T.-Y. Tseng, *Thin Solid Films* 531, 1 (2013).
19. H. Zhang, B. Gao, B. Sun, G. Chen, L. Zeng, L. Liu, Liu, J. Lu, R. Han, J. Kang, and B. Yu, *Appl. Phys. Lett.* 96, 123502 (2010).
20. X. Lu, L. Deng, and J. Du, *J. Non-Cryst. Solids* 491, 141 (2018).
21. J. Du, R. Devanathan, L.R. Corrales, W.J. Weber, and A.N. Cormack, *Phys. Rev. B* 74, 214204 (2006).
22. M. Montorsi, C. Leonelli, M.C. Menziani, J. Du, and A.N. Cormack, *Phys. Chem. Glas.* 43, 137 (2002).
23. M. Hasanuzzaman, A. Rafferty, and A.G. Olabi, *Ceram. Int.* 40, 581 (2014).
24. H. Li, L. Wu, D. u, Wang, Y. Teng, and Y. Li, *J. Nucl. Mater.* 466, 484 (2015).
25. Y.-M. Kuo, K.-L. Huang, C.-T. Wang, and J.-W. Wang, *J. Hazard. Mater.* 169, 626 (2009).
26. Y.-M. Kuo, C.-T. Wang, J.-W. Wang, and K.-L. Huang, *J. Hazard. Mater.* 169, 635 (2009).
27. G.S. Henderson, *Canad. Mineral.* 43, 1921 (2005).
28. S.K. Lee, and J.F. Stebbins, *Geochim. Cosmochim. Acta* 73, 1109 (2009).
29. R.-G. Duan, K.-M. Liang, and S.-R. Gu, *Mater. Chem. Phys.* 57, 92 (1998).
30. S. Fakhfakh, O. Jbara, S. Rondot, A. Hadjadj, J.M. Patat, and Z. Fakhfakh, *J. Appl. Phys.* 108, 093705 (2010).
31. M.A. Villegas, and J.M.F. Navarro, *J. Mater. Sci.* 23, 2464 (1988).
32. E.M.A. Khalil, F.H. ElBatal, Y.M. Hamdy, H.M. Zidan, M.S. Aziz, and A.M. Abdelghany, *Phys. B* 405, 1294 (2010).
33. J.R. Ferraro, and M.H. Manghnani, *J. Appl. Phys.* 43, 4595 (1972).
34. D.E. Clark, M.F. Dillmore, E.C. Ethridge, and L.L. Hench, *J. Am. Ceram. Soc.* 59, 62 (1976).
35. C.B. Amara, H. Hammami, and S. Fakhfakh, *J. Mater. Sci. Mater. Electron.* 30, 13543 (2019).
36. R.B. Rao, N.O. Gopal, and N. Veeraiah, *J. Alloys Compd.* 368, 25 (2004).
37. H.A. Abo-Mosallam, D.A. Kim, H.-W. Kim, and H.H. Lee, *Ceram. Int.* 42, 5107 (2016).
38. A. Quintas, D. Caurant, O. Majérous, P. Loiseau, T. Charpentier, and J.-L. Dussossoy, *J. Alloys Compd.* 714, 47 (2017).
39. S.V. Trukhanov, L.S. Lobanovski, M.V. Bushinsky, V.A. Khomchenko, N.V. Pushkarev, I.O. Troyanchuk, A. Maignan, D. Flahaut, H. Szymczak, and R. Szymczak, *Eur. Phys. J. B* 42, 51 (2004).
40. S.V. Trukhanov, A.V. Trukhanov, and H. Szymczak, *Low Temp. Phys.* 37, 465 (2011).
41. M.V. Zdorovets, and A.L. Kozlovskiy, *Ceram. Int.* 46, 14548 (2020).
42. S.V. Trukhanov, A.V. Trukhanov, H. Szymczak, R. Szymczak, and M. Baran, *J. Phys. Chem. Solids* 67, 675 (2006).
43. M.V. Zdorovets, I.E. Kenzhina, V. Kudryashov, and A.L. Kozlovskiy, *Ceram. Int.* 46, 10521 (2020).
44. M. Ficheux, E. Burov, L. Cormier, E. Gouillart, and N. Trcera, *Geochim. Cosmochim. Acta* 270, 394 (2020).
45. F. Farges, and G. Calas, *Am. Mineral.* 76, 60 (1991).
46. J.B. Charles, and F.D. Gnanam, *Cryst. Res. Technol.* 29, 707 (1994).
47. N. Kanagathara, N.G. Renganathan, M.K. Marchewka, N. Sivakumar, K. Gayathri, P. Krishnan, S. Gunasekaran, and G. Anbalagan, *Acta A Mol. Biomol. Spectrosc.* 101, 112 (2013).
48. A.V. Trukhanov, N.A. Algarou, Y. Slimani, M.A. Almessiere, A. Baykal, D.I. Tishkevich, D.A. Vinnik, M.G. Vakhitov, D.S. Klygach, M.V. Silibin, T.I. Zubar, and S.V. Trukhanov, *RSC Adv.* 10, 32638 (2020).
49. A.L. Kozlovskiy, and M.V. Zdorovets, *Compos. B Eng.* 191, 107968 (2020).
50. D.A. Vinnik, F.V. Podgornov, N.S. Zabeivorota, E.A. Trofimov, V.E. Zhivulin, A.S. Chernukha, M.V. Gavriilyak, S.A. Gudkova, D.A. Zherebtsov, A.V. Ryabov, S.V. Trukhanov, T.I. Zubar, L.V. Panina, S.V. Podgornaya, M.V. Zdorovets, and A.V. Trukhanov, *J. Magn. Magn. Mater.* 498, 166190 (2020).
51. A.V. Trukhanov, K.A. Astapovich, M.A. Almessiere, V.A. Turchenko, E.L. Trukhanova, V.V. Korovushkin, A.A. Amirov, M.A. Darwish, D.V. Karpinsky, D.A. Vinnik, D.S. Klygach, M.G. Vakhitov, M.V. Zdorovets, A.L. Kozlovskiy, and S.V. Trukhanov, *J. Alloys Compd.* 822, 153575 (2020).
52. K. Funke, R.D. Banhatti, S. Brückner, C. Cramer, C. Krieger, A. Mandanici, C. Martiny, and I. Ross, *Phys. Chem. Chem. Phys.* 4, 3155 (2002).
53. D.E. Day, *J. Non-Cryst. Solids* 21, 343 (1976).
54. A.K. Varshneya, *Fundamentals of Inorganic Glasses* (Amsterdam: Elsevier, 2013).
55. K.M. Shaju, and S. Chandra, *Phys. Status Solidi B.* 181, 301 (1994).
56. D. Johnson, *ZPlot, ZView Electrochemical Impedance Software, Version 2.3 b*, Scribner Associates Inc., North Carolina (2000).
57. J. Jiang, T.J. Zhang, B.S. Zhang, and H. Mao, *J. Electroceramics* 21, 258 (2008).
58. S.G. Song, Z. Ling, and F. Placido, *Mater. Res. Bull.* 40, 1081 (2005).
59. H. Scholze, *Glass-Nature Structure and Properties* (New York: Springer-Verlag, 2012).

Publisher's Note Springer Nature remains neutral with regard to jurisdictional claims in published maps and institutional affiliations.